ADVANCED ENERGY MATERIALS
www.advenergymat.de

Kesterite Thin-Film Solar Cells: Advances in Materials Modelling of Cu_2ZnSnS_4

Aron Walsh, Shiyou Chen, Su-Huai Wei, and Xin-Gao Gong*

Quaternary semiconducting materials based on the kesterite (A_2BCX_4) mineral structure are the most promising candidates to overtake the current generation of light-absorbing materials for thin-film solar cells. Cu_2ZnSnS_4 (CZTS), $Cu_2ZnSnSe_4$ (CZTSe) and their alloy $Cu_2ZnSn(Se,S)_4$ consist of abundant, low-cost and non-toxic elements, unlike current CdTe and $Cu(In,Ga)Se_2$ based technologies. Zinc-blende related structures are formed by quaternary compounds, but the complexity associated with the multi-component system introduces difficulties in material growth, characterization, and application. First-principles electronic structure simulations, performed over the past five years, that address the structural, electronic, and defect properties of this family of compounds are reviewed. Initial predictions of the bandgaps and crystal structures have recently been verified experimentally. The calculations highlight the role of atomic disorder on the cation sub-lattice, as well as phase separation of Cu_2ZnSnS_4 into ZnS and $CuSnS_3$, on the material performance for light-to-electricity conversion in photovoltaic devices. Finally, the current grand challenges for materials modeling of thin-film solar cells are highlighted.

1. Introduction

Sunlight is the most abundant natural energy source, and light-to-electricity conversion in solar cells is one of the best-developed renewable energy technologies. Conversion efficiencies for single-junction photovoltaic devices are approaching their limit of ca. 30%, and the performance of multi-junction devices can now exceed 43%.[1] The limiting factors that will emerge as the demand for solar cells reaches towards the terawatt scale are material cost and availability, as well as the scaling-up of device fabrication.[2]

Since the commercialization of Si solar cells in the 1950s, the search for alternative light-absorbing materials has been an active area of research. Replacing Si, which has an indirect bandgap and hence a low optical absorption coefficient, with a material with a high absorption coefficient (direct bandgap) enables the fabrication of second-generation thin-film solar cells at much lower economic and energetic cost.[3] If such a material was composed of earth abundant elements, then a solar cell could be manufactured sustainably to meet all future market demands. Two principal thin-film technologies have emerged in the past decades based on CdTe[4,5] and $Cu(In, Ga)Se_2$ (CIGS).[6–9] These devices have advanced to light-to-electricity conversion efficiencies close to 20%, which are comparable to their Si counterparts.[1] Thin-film solar cell devices are currently been produced in the hundreds of megawatt range; however, as this volume increases to the gigawatt level, the cost and scarcity of In and Te,[10] as well as the toxicity of Cd, will become major issues that could limit the widespread utilization of second-generation photovoltaics.[3]

The search and optimization of alternative thin-film materials is an ongoing and active area of research.[11] The material selection criteria includes the following:

- Semiconducting properties: robust *p*-type and/or *n*-type conductivity.
- Strong optical absorption coefficient (direct bandgap of ~1.5 eV).
- Low-cost and abundant chemical elements.
- Low-cost material growth.
- Compatible with existing technologies: structures and work-function.

To meet all of these criteria, moving from binary and ternary to more complex materials offers a greater degree of freedom. Following the early work of Ito and Nakazawa,[12] over the past five years, the study of the quaternary chalcogenide

A. Walsh
Centre for Sustainable Chemical Technologies
and Department of Chemistry
University of Bath
Claverton Down, Bath BA2 7AY, UK
E-mail: a.walsh@bath.ac.uk
S. Chen, X.-G. Gong
Key Laboratory for Computational Physical Sciences (MOE)
Fudan University
Shanghai 200433, China
S. Chen, X.-G. Gong
Surface Physics Laboratory
Fudan University
Shanghai 200433, China
S. Chen
Key Laboratory of Polar Materials and Devices (MOE)
East China Normal University
Shanghai 200241, China
S.-H. Wei
National Renewable Energy Laboratory
Golden, Colorado 80401, USA

DOI: 10.1002/aenm.201100630

semiconductor Cu_2ZnSnS_4 (CZTS) for solar cells has intensified, because the material combines an optimal bandgap of 1.5 eV and a high optical absorption coefficient of 10^4 cm^{-1} (for an example of the literature, see references[13–23]). Compared to the current range of thin-film solar cell absorbers, the advantage of CZTS is that all of the constituent elements are naturally abundant and non-toxic, thus facilitating large-area production. Furthermore, the conversion efficiency of CZTS based solar cells recently reached 10%.[16,24] However, with complex multinary materials, issues arise concerning crystal structure, stoichiometry, point defect behaviour, morphology and their relationship to photovoltaic performance. These issues are gradually being resolved for the CZTS system through a combination of experimental synthesis, characterization and electronic structure calculations.

In this paper, we review recent computational work concerning the materials chemistry and physics of kesterite-based compounds, which is placed in the context of the latest experimental studies. The majority of theoretical studies have been performed within the framework of density functional theory[25,26] (DFT), which is an ab initio quantum mechanical method that can be used to calculate the total energy and electronic structure of metals, semiconductors and insulating materials.[27] A number of material issues are identified, which when overcome, will help to close the gap in conversion efficiency between Cu_2ZnSnS_4 based thin-film solar cells and more mature technologies. The work on Cu_2ZnSnS_4 also highlights the powerful role of materials modeling in the design and optimization of novel functional materials systems.

2. Cation Mutation (Cross-Substitution) in Tetrahedral Semiconductors

The formation of stoichiometric multi-component semiconductors can be considered as a sequential process involving a series of cation mutations (cross-substitutions) in which the overall valence state is maintained and the compound remains charge neutral. For example, two 3^+ ions [III_2] have an equivalent charge to one 2^+ and one 4^+ ion [II–IV] or one 1^+ and one 5^+ [I–V]. The fundamental theory of this process was developed by Goodman and Pamplin in the 1950s and 60s,[28,29] following the earlier models of Pauling[30] and Lewis.[31,32] A schematic of the cross-substitution steps required to form I_2–II–IV–VI_4 compounds is shown in **Figure 1**.

The binary II–VI semiconductors adopt the cubic zinc-blende (or hexagonal wurtzite) structure in which there are two interpenetrating fcc networks and both the group II and VI atoms have tetrahedral coordination environments. The ternary I–III–VI_2 compounds can be generated by mutating the group II atoms into pairs of group I and III atoms. This progression introduces the possibility of cation ordering: the lowest energy structures are those where the group I and III atoms are ordered in (201) (the chalcopyrite structure) and (001) (the CuAu structure) planes.[33] These structures are favoured as they satisfy the condition of local charge neutrality,[34] i.e., each anion is coordinated to two group I and two group III cations (see **Figure 2**). Relative to the parent binary compounds, the ternary semiconductors exhibit more flexible properties arising

Aron Walsh is a Royal Society University Research Fellow at the University of Bath. He obtained his PhD in Chemistry from Trinity College Dublin in 2006 and has since worked at the National Renewable Energy Laboratory and University College London. His research focuses on the development and application of computational techniques for functional materials design and characterisation.

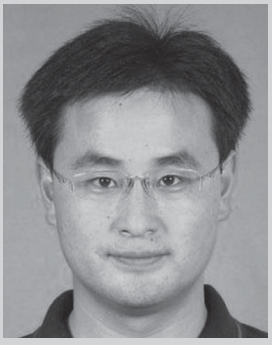

Shiyou Chen is an Associate Professor in the Department of Electronic Engineering and the Key Laboratory for Polar Materials and Devices, East China Normal University. He obtained his PhD in Condensed Matter Physics from Fudan University in 2009. His research focuses on the calculation study of the multi-component semiconductors for photovoltaic and photocatalytic applications.

Su-Huai Wei received his PhD from the College of William and Mary in 1985. He joined the National Renewable Energy Laboratory in 1985 and is currently a Principal Scientist and Manager for the Theoretical Materials Science Group. His research is focused on developing electronic structure theory of materials, especially for energy applications. He is a Fellow of the American Physical Society.

Xingao Gong received his PhD from the Institute of Solid State Physics, Chinese Academy of Sciences, in 1993. He joined Fudan University in 2000 and is currently a Xie Xide Chair Professor of Physics, and also Director of the Key Laboratory of Computational Physical Sciences, Ministry of Education. His research is focused on computational studies of the structural and electronic properties of materials. He is a fellow of the American Physical Society.

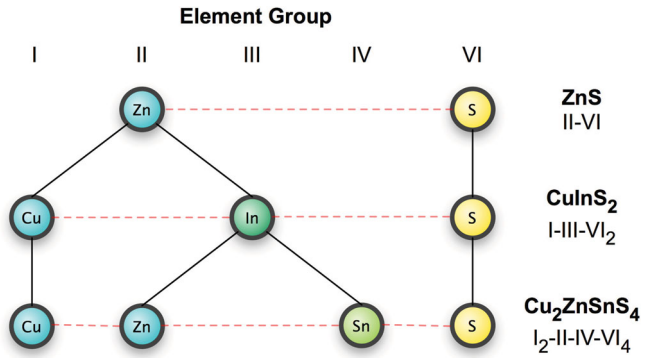

Figure 1. Relationship between binary, ternary, and quaternary semiconductors to produce Cu_2ZnSnS_4, starting from a II–VI parent compound.

from their enhanced chemical and structural freedom, e.g., the bandgap of $CuGaSe_2$ (1.68 eV) is lower than ZnSe (2.82 eV) and is more suitable for application in thin-film solar cells, especially when alloyed with $CuInSe_2$ to lower the gap further.

One route to designing novel materials is to follow the mutation concept to further split the ternary I–III–VI_2 systems into quaternary compounds (see Figure 1). There are two methods for this cation mutation: (i) to replace two group III atoms by one group II and one group IV atom, forming a I_2–II–IV–VI_4 compound; (ii) to replace one group I atom and one III by two II atoms, forming a I–III–II_2–VI_4 compound. Through this ternary-to-quaternary mutation and control of the atomic configuration, one can perform band engineering to tailor the material properties for a specific application. Indeed by screening a large number of possible compositions,[35] this family of materials contains systems that have been predicted to be optimal for solar cell,[36] spintronic[37] and thermoelectric[38] applications, as well as a new class of topological insulator.[39]

For the quaternary compounds, similar tetrahedral crystal structures are maintained to their parent materials. The structural progression from binary to quaternary semiconductor is shown in Figure 2. The possibility for cation ordering is present, with the complexity of the problem increasing to three lattice sites for the quaternary material, e.g., Cu, Zn and Sn in CZTS. However, the condition of local charge neutrality again restricts the number of thermodynamically accessible low energy phases. Two of the crystal structures naturally occur: (i) the mineral kesterite $Cu_2(Zn,Fe)SnS_4$ (space group $I\bar{4}$), (ii) the mineral stannite Cu_2FeSnS_4 (space group $I\bar{4}2m$). These are two structurally similar, but distinct crystal structures[40] that differ in the ordering of the I_2–II sublattice: kesterite is derived from the chalcopyrite (201) ordering and stannite is derived from the CuAu (001) ordering, as shown in Figure 2A third type of ordering can be derived from the CuAu structure, PMCA (space group $P\bar{4}2$ m), which features a 90° rotation in one of the II–IV layers, but to our knowledge has never been reported experimentally.

It should also be noted that following the relationship between the fcc zincblende and hcp wurtzite crystal structures, hexagonal polytypes of the ternary and quaternary crystal structures can also exist. The structural preference is controlled by cation size and ionicity, with the hexagonal structures generally preferred by the more polarizable Ag and Cd containing materials.[41] While the electronic properties (bandgaps and valence band alignments) are similar for the hexagonal and cubic systems, the small energy difference between the two polytypes introduces the possibility of more complex stacking faults in direct analogy to the SiC system,[42] although no experimental or theoretical studies have addressed this issue thus far.

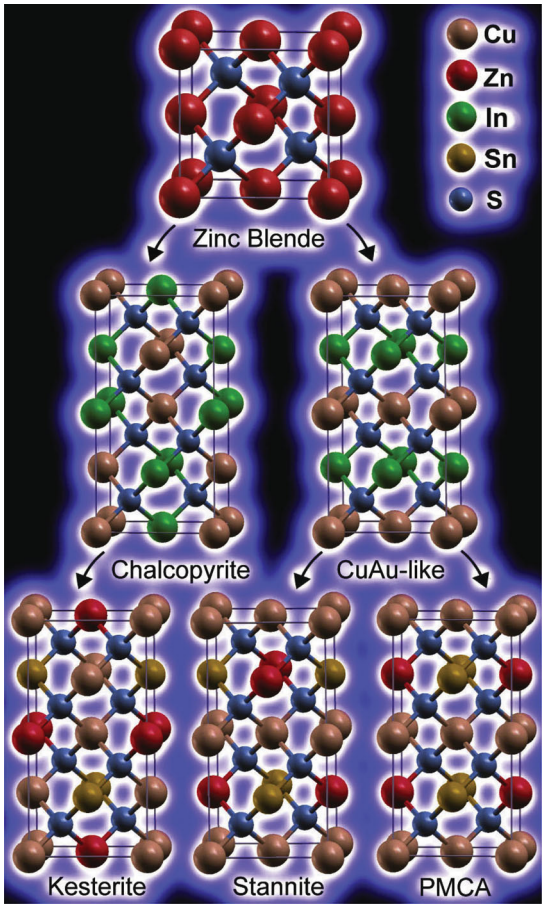

Figure 2. Crystal structure representations of zinc-blende ZnS; (201) ordered chalcopyrite $CuInS_2$; (001) ordered CuAu-like $CuInS_2$; kesterite Cu_2ZnSnS_4; stannite Cu_2ZnSnS_4, and mixed-CuAu Cu_2ZnSnS_4.

3. Cu_2ZnSnS_4: Bulk Structural and Electronic Properties

Cu_2ZnSnS_4 can be derived from $CuInS_2$ by replacing two In atoms by one Zn and one Sn; hence its crystal and electronic structures inherit certain characteristics from $CuInS_2$. Due to the similarity between CZTS and $CuInSe_2$, CZTS-based solar cells can be used in a comparable device architecture to CIGS solar cells, and it is expected that CZTS will substitute CIGS in the future, once the solar to electricity conversion efficiency is competitive. Recently, the photocatalytic activity of CZTS has been reported for the water-splitting reaction,[43] as well as its application as an electrode in dye-sensitized solar cells.[44]

Table 1. Survey of density functional theory calculations of the structural properties and bandgap of Cu_2ZnSnS_4. The acronyms in the method column refer to the type of exchange-correlation functional used in the calculation, i.e., the local density approximation (LDA),[63] the generalized gradient approximation (GGA),[64] a screened hybrid method (HSE),[47] or to the level of many-body perturbation theory[48] including non-self-consistent (G_0W_0) or self-consistent (scGW) approaches. The predictions are compared to neutron diffraction measurements (crystals from a solid-state reaction)[15] and optical absorption measurements (thin-films from electrochemical deposition).[13] Note that the kesterite structure is a $1 \times 1 \times 2$ tetragonal expansion of zincblende, and the tetragonal distortion can be quantified by the lattice vector ratio $c/2a$.

Study	Method	Reported Stable Phase	a [Å]	$c/2a$	E_g [eV]
Chen ('09)[35,57]	GGA (HSE)	Kesterite	5.467	0.999	0.09 (1.50)
Paier ('09)[58]	GGA (HSE)	Kesterite	5.466	1.000	0.10 (1.49)
Ichimura ('09)[59]	GGA	Kesterite	5.51	1.02	-
Amiri ('10)[46]	LDA	-	5.639	0.996	0.03
Zhang ('11)[60]	GW(+U)+G0W0	-	-	-	1.08 (1.57)
Zhao ('11)[61]	HSE (+G0W0)	-	-	-	1.39 (1.57)
Botti ('11)[62]	HSE (+scGW)	-	-	-	1.52 (1.64)
Experiment	-	Kesterite	5.428[15]	1.001[15]	1.49[13]

3.1. Crystal Structure

Experimentally, CZTS has been reported to crystallize in both the kesterite and stannite crystal structures. Neutron diffraction measurements by Schorr et al. also showed that a partially-disordered kesterite structure can exist, in which the atoms in the Cu/Zn (001) layer are disordered, while atoms in the Cu/Sn (001) layer reside in their original positions.[15] The results of electronic structure calculations, all based on DFT but with different types of exchange-correlation functional that describe quantum mechanical interaction between electrons in the system, are collected in **Table 1**. The general consensus is that kesterite CZTS is the ground-state structure, which is also obtained from calculation of the relative Madelung energies,[45] but the energy difference between kesterite and stannite (ca. 3 meV per atom) is small, indicating that disorder in the cation sublattice may occur under standard growth conditions. The disorder is predicted to affect the bandgap of the material by 0.15 eV, with the ground-state kesterite phase having the largest electronic bandgap of 1.5 eV.

Due to the large chemical and size mismatch between Cu and Sn, appreciable disorder is only possible on the Cu–Zn sublattice. As illustrated in Figure 2, the kesterite structure has an ordering of cations in (001) planes, which can be expressed as repeating layers of/Cu+Zn/Cu+Sn/Zn+Cu/Sn+Cu/. In a <001> oriented supercell of the kesterite structure, if Zn and Cu in some of the Cu+Zn layers are exchanged, i.e., the atoms in the layers are shifted by $<½, ½, 0> \times a$, this new structure still obeys the valence octet rule, so the total energy change is very small, which is confirmed by electronic structure calculations.[36] If the displacement occurs randomly in the Cu+Zn layers, the disordered kesterite phase results in an effective symmetry equivalent to the stannite structure. However, it is difficult to assign the crystal structure based on X-ray diffraction techniques alone: the difference in the scattering cross-sections between Cu and Zn is small, and hence similar diffraction patterns are produced for kesterite, stannite and all related partially disordered phases.[41] While the vibrational spectra of the two materials are also similar, the change in lattice symmetry results in a appreciable difference in Raman intensities, which have been recently calculated and may be of benefit for future experimental structure characterization.[46]

3.2. Electronic Structure

Calculation of the electronic band structure of CZTS reveals a direct bandgap at the gamma point of the Brillouin zone. While standard DFT calculations at the level of the local density approximation (LDA) or generalized gradient approximation (GGA) grossly underestimate the bandgaps of semiconductors (see Table 1 for CZTS), calculations using hybrid functionals mixed with Hartree-Fock exchange (e.g., HSE[47]) or at the level of many-body perturbation theory (e.g., GW[48]) converge to results around 1.5 eV, which is in good agreement with optical absorption measurements on high quality samples. The prediction of quantitative bandgaps for new materials remains one of the major challenges in computational materials science.[49–52]

The magnitude of the bandgap of CZTS can be understood according to the chemical nature of the valence and conduction band states, and in particular, the low binding energy of the filled Cu 3d valence band. The natural band alignments, calculated with reference to the energy difference of deep atomic-like core states across a material heterojunction,[53] are plotted in **Figure 3** for a range of common solar cell materials. For all Cu based chalcogenides, including the quaternary and ternary compounds, the valence band maximum (VBM) is an antibonding state of the anion p and Cu d orbitals.[33] The valence p level of S is lower in energy than Se, thus the VBM of the sulfides is lower than that of the selenides; e.g., the VBM is 0.52 eV lower for ZnS than ZnSe,[53] but the difference is reduced by anion p–Cu d overlap (p-d hybridization) in Cu based chalcogenides, because the hybridization is stronger in the shorter Cu–S bond and pushes the antibonding VBM level of the sulfide up relative to that of the selenide. As a result, the valence band offset between the sulphides and selendies is less than 0.2 eV. In contrast, the lower conduction band is controlled by the metal s states, and for CZTS this is predominately the Sn 5s orbital.

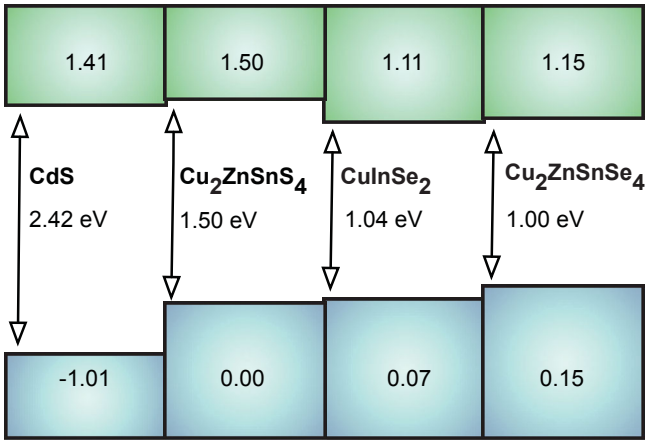

Figure 3. The calculated band alignment between CdS, Cu_2ZnSnS_4, $Cu_2ZnSnSe_4$ and $CuInSe_2$ (adapted from Ref. [65]). CdS is a commonly used *n*-type window layer in thin-film solar cells.

Following the phenomenological doping limit rules of semiconductors,[54–56] the high valence band level should result in good *p*-type conductivity for all Cu(I)-based compounds.

4. Cu_2ZnSnS_4: Phase Competition and Separation

An important issue with quaternary semiconductors is whether homogeneous samples can be synthesized experimentally, or if secondary phases are also unintentionally formed. CZTS samples have been grown successfully using a variety of techniques (vacuum and non-vacuum; solution and solid-state), and significant variation can be achieved in the Cu:Zn:Sn atomic ratio, depending on the growth environment.[66] To describe theoretically the phase stability of CZTS relative to the secondary compounds, the stability region in the atomic chemical potential space has been calculated,[67,68] as shown in **Figure 4**.

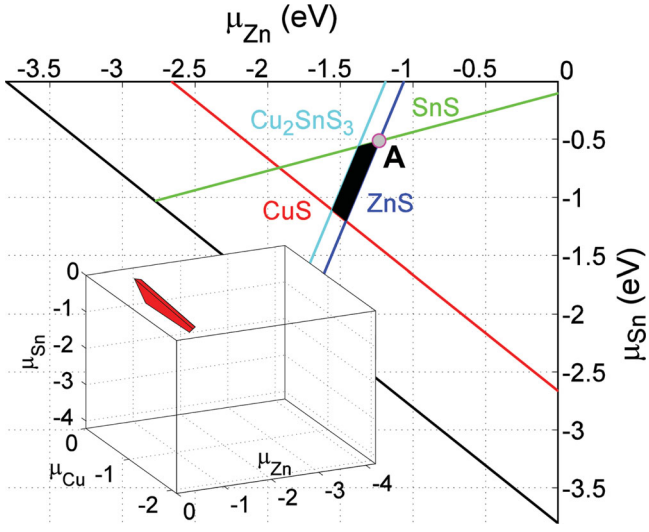

Figure 4. The calculated chemical-potential stability diagram[67,68] of Cu_2ZnSnS_4 in a 2D Cu-rich plane (the stable 3D region is inset). All values are in eV.

The thermodynamic chemical potential μ_i can be introduced to describe the abundance of an element *i*. The limit of $\mu_i = 0$ means the particular element is in equilibrium with its standard state (gas, liquid, or solid). Since the pure Cu, Zn, Sn metals and S, Se bulk are not allowed to exist in the synthesized stoichiometric samples, the atomic chemical potentials are required to be negative. In addition to the elemental standard states, secondary phases such as CuS, ZnS, SnS and Cu_2SnS_3 (similarly for selenides) are also in competition, thus the following relations must be satisfied to avoid their formation for CZTS:

$$\mu_{Cu} + \mu_S < \Delta H_f(CuS) = -0.49eV$$

$$2\mu_{Cu} + \mu_S < \Delta H_f(Cu_2S) = -0.52eV$$

$$\mu_{Zu} + \mu_S < \Delta H_f(ZnS) = -1.75eV$$

$$\mu_{Su} + \mu_S < \Delta H_f(SnS) = -1.01eV$$

$$\mu_{Sn} + 2\mu_S < \Delta H_f(SnS_2) = -1.33eV$$

$$2\mu_{Cu} + \mu_{Sn} + 3\mu_S < \Delta H_f(Cu_2SnS_3) = -2.36eV$$

where ΔH_f represents the calculated formation enthalpy of each compound from their elemental standard states. To maintain a stable Cu_2ZnSnS_4 crystal, the chemical potentials of Cu, Zn, Sn, and S must satisfy the following equation:

$$2\mu_{Cu} + \mu_{Zn} + \mu_{Sn}\ 4\mu_S = \Delta H_f(Cu_2ZnSnS_4) = -4.21eV.$$

Under the established constraints, the chemical-potential range of Cu, Zn, and Sn that stabilizes CZTS is bound in a polyhedron in the 3D (μ_{Cu}, μ_{Zn}, and μ_{Sn}) space. A slice of the polyhedron in a Cu-rich plane is shown in Figure 4. The black area indicates the stable regions. As we can see, the volume of the stable region is small, and a deviation outside this space will cause the formation of CuS, ZnS, SnS, or Cu_2SnS_3. The narrow thermodynamic window demonstrates that chemical-potential control is important for the growth of high-quality crystals. In particular, the stable region is narrow along the μ_{Zn} axis, thus the control of Zn content is crucial.

Experimentally, ZnS and Cu_2SnS_3 have been observed in the samples, which can be confirmed by Raman scattering analysis,[69] and can be explained according to the narrow accessible range of μ_{Zn}, i.e., Zn-rich leads to ZnS, while Zn-poor leads to Cu_2SnS_3. A recent study has shown that the energy required to phase separate stoichiometric CZTS into ZnS and Cu_2SnS_3 is only of the order of 0.1 eV.[70] With the absence of a high thermodynamic barrier, the kinetics of material growth will play a crucial rule in determining the homogeneity of CZTS samples. A further complication is that the structure of Cu_2SnS_3 is constructed of tetrahedral Cu–S–Sn building blocks, so that the three co-existing phases CZTS, Cu_2SnS_3, and ZnS may be indistinguishable by diffraction techniques, as demonstrated in **Figure 5**. However, the value of the bandgap of Cu_2SnS_3 at ~1 eV[70] is smaller than CZTS, so that a low-cost multi-junction metal sulfide solar cell could be fabricated if the synthesis of each phase can be properly controlled.

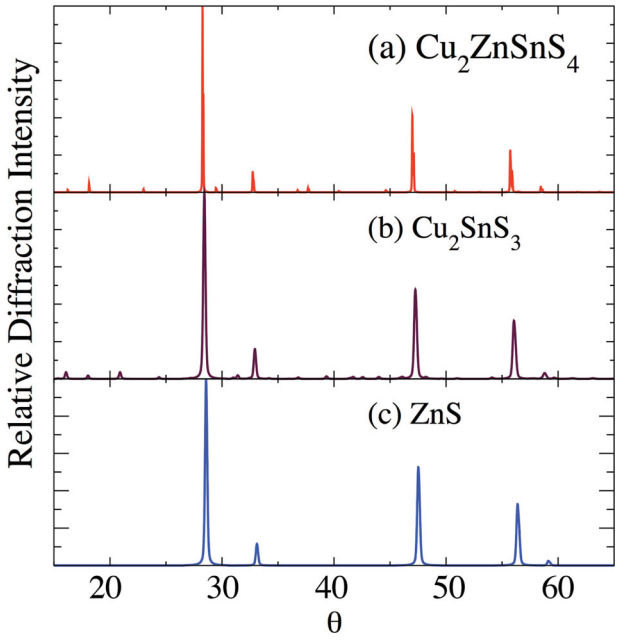

Figure 5. Simulated Cu-Kα X-ray diffraction patterns of kesterite Cu_2ZnSnS_4, Cu_2SnS_3 (spacegroup Cc) and zincblende ZnS. Note the overlap of the main diffraction peaks between the three materials, which is one difficulty for material characterization.

5. Cu_2ZnSnS_4: Point Defect Formation

Beyond the crystal and electronic structure, knowledge of the concentration and properties of lattice defects is also important for explaining the compositional dependence of the solar cell efficiency. These defects can give rise to conductivity (determining equilibrium electron and hole carrier concentrations); colour (absorbing or emitting light) and species with deep states in the electronic bandgap may act as recombination centers for photogenerated electrons and holes. One important factor that leads to the high efficiency of CIGS solar cells is its unique defect microstructure, e.g., intrinsic defects in $CuInSe_2$ undergo self-passivation through the formation of defect complexes such as $[In_{Cu}^{2+}+2V_{Cu}^{-}]$,[71] and the interface between the absorber layer and the CdS layer can be inverted to *n*-type, which facilitates the separation of electron-hole pairs. These special defect properties make CIGS solar cells exhibit good performance, despite the poor crystallinity (small grain sizes) and high levels of non-stoichiometry. As kesterite solar cells are developed, the question arises as to whether their defect physics follows that of $CuInSe_2$.

As a quaternary compound, Cu_2ZnSnS_4 has more possible lattice defects, such as vacancies, antisites and interstitials, than binary or ternary compounds. The equilibrium concentration of point defects in materials is determined by their energy of formation, which is dependent on the atomic thermodynamic chemical potential (growth conditions),[72] as well as the electron chemical potential (Fermi energy)[73,74] for charged defects. The calculated formation energies[67,68] of different lattice defects are shown in **Figure 6**. As the Fermi energy shifts up from the valence to conduction band (i.e., for an increase in the nominal electron carrier concentration), the formation energy of the negatively charged acceptor defects such as V_{Cu}, Cu_{Zn}, and Zn_{Sn} decreases. When the formation energy of a charged defect is lower than that of the neutral (or alternatively charged)

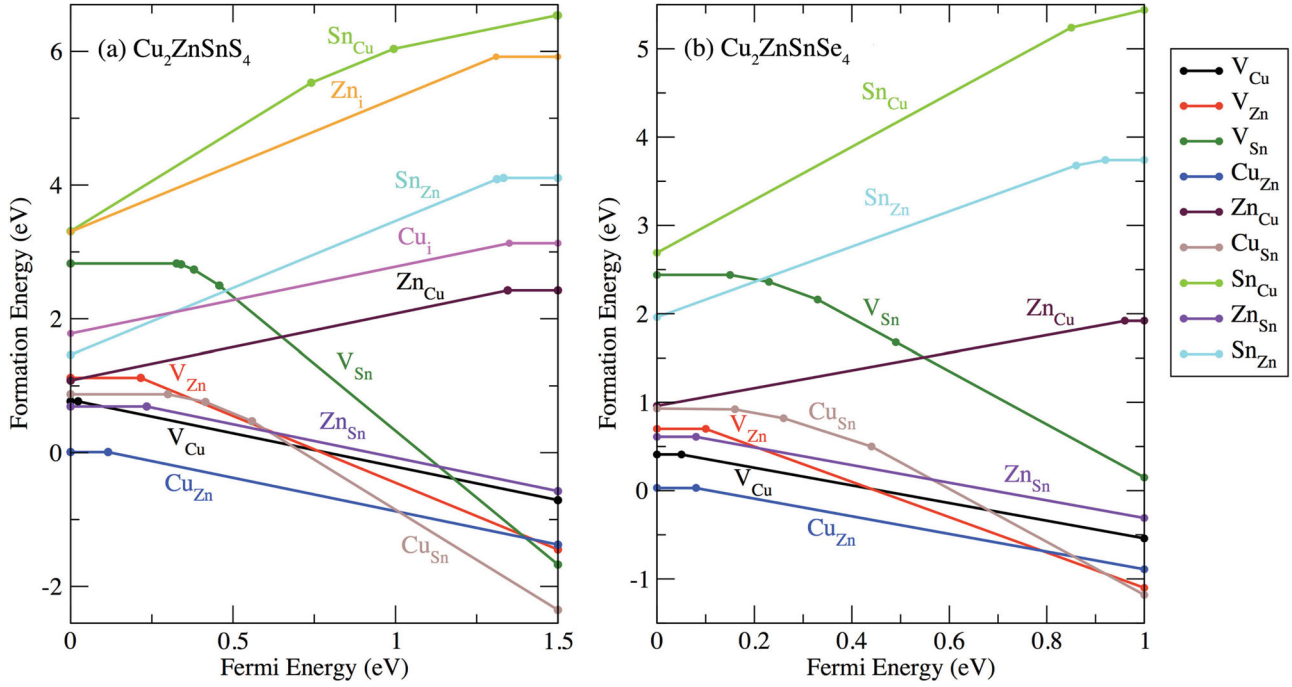

Figure 6. Calculated defect formation energy as a function of the Fermi energy at the thermodynamic chemical-potential point **A** (from Figure 4) for Cu_2SnZnS_4 (adapted from [67,68]). For comparison, the corresponding plot for $Cu_2SnZnSe_4$ is also shown in part (b). For each value of the Fermi energy only the most stable charge state is plotted, with the filled circles (change of slope) representing a change in charge state (transition energy level).

Table 2. Survey of recent density functional theory calculations of point defect formation in Cu_2ZnSnS_4. All values are in eV, and the acceptor levels are given with respect to the top of the valence band.

Study	Method	V_{Cu}: Formation Energy[a)]	V_{Cu}: Acceptor Level[a)]	Cu_{Zn}: Formation Energy[a)]	Cu_{Zn}: Acceptor Level[a)]
Chen ('10)[67,68]	GGA	0.77	0.02	0.01	0.12
Nagoya ('10)[75]	GGA	0.59	0.00	-0.06	0.05
Maeda ('11)[76]	GGA	0.8	-	-	-

[a)]The defect energies are reported in the Cu-rich limit for the neutral defect and the acceptor level (thermodynamic transition level) to form the negatively charged defect is given with respect to the valence band of the bulk material.

one, the position of the Fermi energy relates to a transition energy level (or ionization level), which are shown by filled circles in Figure 6. In contrast to the acceptor defects, the formation energy of positively charged donors, such as Zn_{Cu}, Cu_i, and Sn_{Zn}, increases as the Fermi energy moves towards the conduction band due to the energy penalty associated with additional high-energy electron carriers.

From Figure 6, two results are clear: (i) the formation energies of most acceptor defects are lower than those of donor defects, explaining the experimentally observed *p*-type conductivity and indicating that *n*-type doping will be difficult in these compounds; (ii) the lowest energy defect (for the assumed chemical potentials) is Cu_{Zn} antisite, which is different from the case of $CuInSe_2$ where the dominant defect is the Cu vacancy. As the energy difference for other acceptors (V_{Cu}, V_{Zn}, Zn_{Sn}, Cu_{Sn}) relative to the dominant Cu_{Zn} is not very large (less than 1 eV), these defects may also be present in much smaller concentrations. Three computational defect studies[67,75,76] of Cu_2SnZnS_4 agree on a formation energy of the copper vacancy of between 0.6–0.8 eV, and a value of the copper vacancy close to 0 eV (shallow acceptor) under copper-poor conditions (see **Table 2**). The relative concentrations can be tuned by controlling the material growth conditions (atomic chemical potentials).

The calculated ionization levels of point defects in the bandgap of Cu_2ZnSnS_4, which can be derived from Figure 6a, are shown more clearly as vertical plots in **Figure 7**. It is important to note that the dominant defect Cu_{Zn} has an acceptor level 0.12 eV above valence band, deeper than that of V_{Cu} (0.02 eV above VBM). The shallow level of V_{Cu} is common in Cu-based chalcopyrites like $CuInSe_2$ and $CuGaSe_2$.[71,77] The deeper level of Cu_{Zn} can be explained by considering that the Cu on Zn antisite enhances the p–d hybridization between Cu and S. Low temperature photoluminescence measurements of CZTS identified two shallow acceptor states (10 and 30 meV above the VBM),[78] which could be attributed to two symmetry inequivalent Cu vacancy sites. The deep level of the dominant antisite defect is negative for CZTS solar cell efficiency, as it will decrease the open-circuit voltage. Therefore, it should be beneficial to decrease the formation energy and enhance the population of shallow V_{Cu} relative to Cu_{Zn} using Cu-poor and Zn-rich growth conditions. Experimentally this condition has been found to give high solar cell efficiency.[16]

6. $Cu_2ZnSn(S,Se)_4$: Alloy Formation

In addition to CZTS, the corresponding selenide material $Cu_2ZnSnSe_4$ (CZTSe) is also of interest for solar cell applications. Although Se is less abundant than S, it is available at relatively low cost as a side product from mining of metal ores.

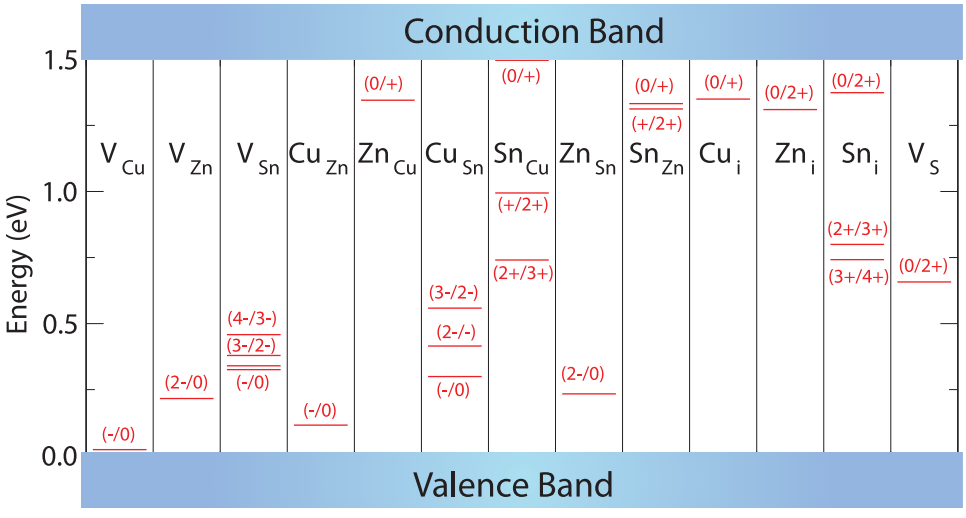

Figure 7. The ionization levels of intrinsic defects in the bandgap of Cu_2ZnSnS_4 (adapted from Ref. [68]). The copper vacancy results in a shallow acceptor level just above the valence band, while the Cu-on-Zn antisite results in a level 0.12 eV higher in energy.

CZTSe adopts the same crystal structure (also with Cu–Zn disorder[79]) but has a smaller bandgap, which was recently predicted[36] and measured[80] to be 1.0 eV. Many earlier students assumed or reported a bandgap of 1.5 eV for CZTSe, which is the same as CZTS, but this higher value is now accepted to be incorrect.[80] A $Cu_2ZnSn(S,Se)_4$ (CZTSSe) thin-film solar cell has achieved a conversion efficiency as high as 10%, which is currently the highest efficiency of kesterite related solar cells.[16] More recently, a CZTSSe nanocrystal based solar cell was reported with an efficiency 7.2%,[81] which is much higher than the efficiency of CZTS nanocrystal cells. This indicates that the addition of Se to CZTS can help the photovoltaic performance; however, the reason is not clear because CZTS itself has an optimal bandgap for visible light conversion. This problem has been approached through explicit calculations of the sulfur–selenium alloy,[65] and subsequent experimental analysis.[17]

The enthalpy of mixing for the sulphur-selenide alloy was calculated using the special quasi-random structure method[82] in conjunction with DFT calculations. The enthalpy can be defined from:

$$\Delta H(x) = E(x) - (1-x)E_{CZTS} - xE_{CZTSe}$$

where E_{CZTS} and E_{CZTSe} represent the total energy of pure CZTS and CZTSe in the kesterite structure, and $E(x)$ is the total energy of the alloy with composition x. The alloy is well behaved and can be described within the thermodynamic framework of the regular solution model, irrespective of the cation ordering (i.e., kesterite or stannite):

$$\Delta H(x) = (1-x)\Delta H(0) + x\Delta H(1) + \Omega x(1-x),$$

where Ω is the interaction parameter that describes the energetic cost of mixing, and is calculated to be 26 meV per atom (or 52 meV per mixed-atom) for the kesterite alloy. For In and Ga mixing in CIGS, the value is much larger (176 meV per mixed-atom), which is consistent with the fact that CIGS is prone to phase separation. Within mean-field theory, the miscibility temperature of CZTSSe is less than 300 K, suggesting that it is stable at typical growth temperatures. These predictions have since been confirmed by the facile growth of the CZTSSe alloy over the full compositional range.[17]

The formation of the alloy is thermodynamically allowed, but how will the solid–solution affect the electronic properties of CZTS? In **Figure 8** we plot the bandgaps of $Cu_2ZnSn(S_{1-x}Se_x)_4$ calculated using a hybrid density functional. The bandgap decreases monotonically with the Se content, from 1.5 eV at $x = 0$ to 0.96 eV at $x = 1$. The decrease is almost linear; i.e., the quadratic bandgap bowing parameter is small. Synthesis of the CZTSSe alloy by Haight et al.[17] resulted in an almost linear bandgap dependence in excellent agreement with the predictions. The calculated bandgap bowing (0.07 eV) of $Cu_2ZnSn(S_{1-x}Se_x)_4$ is similar to those of other mixed-anion alloys, $CuGa(S_{1-x}Se_x)_2$ (0.07 eV) and $CuIn(S_{1-x}Se_x)_2$ (0.04 eV), which results from the small size and chemical differences between S and Se in tetrahedral semiconductors.

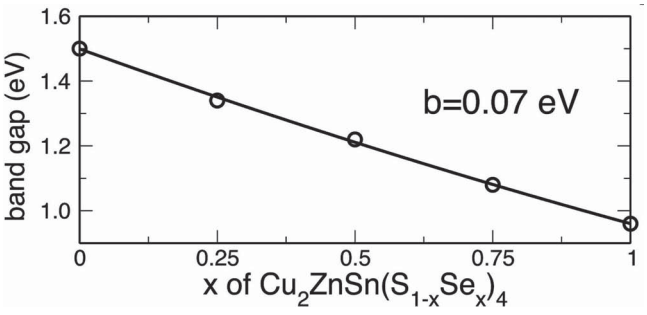

Figure 8. The calculated bandgap of $Cu_2ZnSn(S_{1-x}Se_x)_4$ at different compositions (x) using the hybrid HSE function (adapted from Ref [65]).

To understand in what way the bandgap decreases from CZTS to CZTSe, we can refer to the calculated band offset. As shown in Figure 3, the band alignment between CZTSe and CZTS is of type I; that is, the valence band is higher and the conduction band is lower for the selenide compared to the sulfide. From the larger conduction band offset (0.35 eV) than the valence band offset (0.15 eV), we expect that as the Se content increases in the $Cu_2ZnSn(S_{1-x}Se_x)_4$ alloy, the CBM downshift plays a more important role than the VBM upshift in the bandgap decrease. As the bandgap bowing is small, it is expected that the shift of band edge states is linear as a function of the composition x. The calculated band alignment and estimated band edge shift with the composition offer basic parameters for the device simulation of CZTSSe based solar cells.

A comparison of the energetics of defect formation in Cu_2ZnSnS_4 and $Cu_2ZnSnSe_4$ (Figure 6a,b) reveal that they have similar properties, i.e., acceptor defects have lower formation energy than donors, and Cu_{Zn} antisite is dominant with a deeper acceptor level. However, there are also notable differences: (i) the acceptor level for the antisite defect is relatively shallower in $Cu_2ZnSnSe_4$, because p–d hybridization between Cu and Se is weaker and its valence band is higher; (ii) *n*-type doping should be easier in $Cu_2ZnSnSe_4$. For *n*-type doping of I–III–VI_2 chalcopyrites, it has been shown that the Fermi energy level is pinned at about 0.06 eV above the CBM of $CuInSe_2$, indicating that a I–III–VI_2 semiconductor will be difficult to be doped to *n*-type if its conduction band is much higher than this pinning level. Since kesterite Cu_2ZnSnS_4 and $Cu_2ZnSnSe_4$ have a similar electronic structure to the chalcopyrites, if we assume that the Fermi energy pinning level lines up for all chalcopyrite and kesterite compounds, then it should be possible to dope $Cu_2ZnSnSe_4$ to *n*-type. If the prediction is correct, then type-inversion to *n*-type conduction should be possible at the surface of the *p*-type $Cu_2ZnSnSe_4$ absorber layer, which would facilitate electron–hole separation of photo-generated carriers. Both the shallower acceptor level and more facile *n*-type doping are positive factors for solar cell efficiency, which offers an explanation to the observed high efficiency of CZTSSe alloy-based solar cells.

7. Challenges and Conclusions

Progress in the understanding of kesterite materials and their application in solar cell devices have developed rapidly over the past few years. We have reviewed the major contributions from first-principles calculations relating to the crystal and electronic structure, phase stability and defect properties of Cu_2ZnSnS_4 and related compounds. The results emphasize the delicate interplay between crystal structure and atomic disorder in the quaternary systems; the critical role of secondary phase

formation and the prospect for material engineering through alloy formation.

The entire body of materials modeling for kesterites thus far has related to the characterization of intrinsic bulk material properties, and the challenge now stands to extend this work towards an atomistic description of material heterostructures and thin-film microstructure. In chalcopyrite thin-film solar cells, grain boundaries are known to influence the open-circuit voltage,[83] and first-principles calculations have also been recently applied to assess the role of the Cu vacancy and interstitial diffusion on the creation of p–n junctions and Fermi level pinning.[84,85] The development of atomistic models and knowledge of the electronic structure of these more complex features of kesterite solar cells should be a major goal in the future that would aid in the optimization of device performance. The challenge is to develop large-scale simulation methods that can account for the atomic disorder present at material interfaces, as well as the integration with a grand-canonical model that can describe changes in material/interface structure and stoichiometry as a function of growth conditions (temperature and atomic partial pressures). Finally the time-dependent interaction of light (producing excited electronic states) would allow for direct comparison with optical spectroscopic measurements.

While kesterite compounds represent a viable class of materials for a range of technological applications, many other element combinations and stoichiometries remain to be addressed.[28,29] There have been rapid advancement in the areas of computational crystal structure prediction[45,86–89] and materials design[90–92] both through algorithm development and the utilization of massively parallel supercomputers. By exploiting the increasingly predictive power of materials simulation in the future, the prospect for the identification and development of novel semiconducting materials and systems tailored for energy applications remains bright.

Acknowledgements

AW acknowledges support from the Royal Society for a University Research Fellowship and the European Research Council for a Starting Grant. The work in China has been supported by the Natural Sciences Foundation of China, the Special Funds for Major State Basic Research, and the Research Program of Shanghai municipality and MOE. The work at NREL is funded by the US Department of Energy, under Contract No. DE-AC36-08GO28308.

Received: October 22, 2011
Revised: December 5, 2011
Published online: March 2, 2012

[1] M. A. Green, K. Emery, Y. Hishikawa, W. Warta, *Prog. Photovoltaics: Res. Appl.* **2011**, *19*, 84.
[2] L. M. Peter, *Philos. T. Roy. Soc. A* **2011**, *369*, 1840.
[3] A. Luque, S. Hegedus, *Handbook of Photovoltaic Science and Engineering*, Wiley, Sussex **2011**.
[4] K. Mitchell, A. L. Fahrenbruch, R. H. Bube, *J. Vacuum Sci. Technol.* **1975**, *12*, 909.
[5] D. Cusano, *Solid-State Electronics* **1963**, *6*, 217.
[6] A. Shah, P. Torres, R. Tscharner, N. Wyrsch, H. Keppner, *Science* **1999**, *285*, 692.
[7] A. V. Shah, R. Platz, H. Keppner, *Sol. Energy Mater. Sol. Cells* **1995**, *38*, 501.
[8] L. L. Kazmerski, F. R. White, G. K. Morgan, *Appl. Phys. Lett.* **1976**, *29*, 268.
[9] H. W. Schock, R. Noufi, *Prog. Photovoltaics: Res. Appl.* **2000**, *8*, 151.
[10] V. Fthenakis, W. Wang, H. C. Kim, *Renew. Sust. Energ. Rev.* **2009**, *13*, 493.
[11] C. Wadia, A. P. Alivisatos, D. M. Kammen, *Environ. Sci. Tech.* **2009**, *43*, 2072.
[12] K. Ito, T. Nakazawa, *Jpn. J. Appl. Phys.* **1988**, *27*, 2094.
[13] J. J. Scragg, P. J. Dale, L. M. Peter, G. Zoppi, I. Forbes, *Phys. Stat. Solidi B* **2008**, *245*, 1772.
[14] C. Steinhagen, M. G. Panthani, V. Akhavan, B. Goodfellow, B. Koo, B. A. Korgel, *J. Am. Chem. Soc.* **2009**, *131*, 12554.
[15] S. Schorr, H.-J. Hoebler, M. Tovar, *Eur. J. Mineral.* **2007**, *19*, 65.
[16] T. K. Todorov, K. B. Reuter, D. B. Mitzi, *Adv. Mater.* **2010**, *22*, E156.
[17] R. Haight, A. Barkhouse, O. Gunawan, B. Shin, M. Copel, M. Hopstaken, D. B. Mitzi, *Appl. Phys. Lett.* **2011**, *98*, 253502.
[18] T. Tanaka, T. Nagatomo, D. Kawasaki, M. Nishio, Q. Guo, A. Wakahara, A. Yoshida, H. Ogawa, *J. Phys. Chem. Solids* **2005**, *66*, 1978.
[19] J. S. Seol, S. Y. Lee, J. C. Lee, H. D. Nam, K. H. Kim, *Sol. Energy Mater. Sol. Cells* **2003**, *75*, 155.
[20] H. Katagiri, K. Saitoh, T. Washio, H. Shinohara, T. Kurumadani, S. Miyajima, *Sol. Energy Mater. Sol. Cells* **2001**, *65*, 141.
[21] M. Kurihara, D. Berg, J. Fischer, S. Siebentritt, P. J. Dale, *Phys. Stat. Solidi* **2009**, *6*, 1241.
[22] A. Redinger, S. Siebentritt, *Appl. Phys. Lett.* **2010**, *97*, 092111.
[23] A. Redinger, D. M. Berg, P. J. Dale, S. Siebentritt, *J. Am. Chem. Soc.* **2011**, *133*, 3320.
[24] D. A. R. Barkhouse, O. Gunawan, T. Gokmen, T. K. Todorov, D. B. Mitzi, *Prog. Photovoltaics: Res. Appl.* **2011**, *20*, 6.
[25] W. Kohn, L. J. Sham, *Phys. Rev.* **1965**, *140*, A1133.
[26] P. Hohenberg, W. Kohn, *Phys. Rev.* **1964**, *136*, B864.
[27] M. C. Payne, M. P. Teter, D. C. Allan, T. A. Arias, J. D. Joannopoulos, *Rev. Mod. Phys.* **1992**, *64*, 1045.
[28] C. H. L. Goodman, *J. Phys. Chem. Solids* **1958**, *6*, 305.
[29] B. Pamplin, *J. Phys. Chem. Solids* **1964**, *25*, 675.
[30] L. Pauling, *The Nature of the Chemical Bond*, Cornell University Press, Ithaca **1939**.
[31] N. V. Sidgwick, H. M. Powell, *Proc. R. Soc. A* **1940**, *176*, 153.
[32] G. N. Lewis, *J. Am. Chem. Soc.* **1916**, *38*, 762.
[33] J. Jaffe, A. Zunger, *Phys. Rev. B* **1984**, *29*, 1882.
[34] L. Pauling, *J. Am. Chem. Soc.* **1929**, *51*, 1010.
[35] S. Chen, X. G. Gong, A. Walsh, S.-H. Wei, *Phys. Rev. B* **2009**, *79*, 165211.
[36] S. Chen, X. G. Gong, A. Walsh, S.-H. Wei, *Appl. Phys. Lett.* **2009**, *94*, 041903.
[37] S. Chen, W. J. Yin, J. H. Yang, X. Gong, A. Walsh, S. H. Wei, *Appl. Phys. Lett.* **2009**, *95*, 052102.
[38] C. Sevik, T. Cagin, *Appl. Phys. Lett.* **2009**, *95*, 112105.
[39] S. Chen, X. Gong, C. G. Duan, Z. Q. Zhu, J. H. Chu, A. Walsh, Y. G. Yao, J. Ma, S. H. Wei, *Phys. Rev. B* **2011**, *83*, 245202.
[40] S. Hall, J. Szymanski, J. Stewart, *Can. Mineral.* **1978**, *16*, 131.
[41] S. Chen, A. Walsh, Y. Luo, J. H. Yang, X. Gong, S. H. Wei, *Phys. Rev. B* **2010**, *82*, 195203.
[42] C. H. Park, B. H. Cheong, K. H. Lee, K. J. Chang, *Phys. Rev. B* **1994**, *49*, 4485.
[43] D. Yokoyama, T. Minegishi, K. Jimbo, T. Hisatomi, G. Ma, M. Katayama, J. Kubota, H. Katagiri, K. Domen, *Appl. Phys. Express* **2010**, *3*, 101202.
[44] X. Xin, M. He, W. Han, J. Jung, Z. Lin, *Angew. Chem.* **2011**, *123*, 11943.
[45] C. R. A. Catlow, Z. X. Guo, M. Miskufova, S. A. Shevlin, A. G. H. Smith, A. A. Sokol, A. Walsh, D. J. Wilson, S. M. Woodley, *Phil. Trans. R. Soc. A* **2010**, *368*, 3379.

[46] N. B. Mortazavi Amiri, A. Postnikov, *Phys. Rev. B* **2010**, *82*, 205204.
[47] J. Heyd, G. E. Scuseria, *J. Chem. Phys.* **2004**, *121*, 1187.
[48] L. Hedin, *Phys. Rev.* **1965**, *139*, A796.
[49] E. N. Brothers, A. F. Izmaylov, J. O. Normand, V. Barone, G. E. Scuseria, *J. Chem. Phys.* **2008**, *129*, 011102.
[50] F. Corà, M. Alfredsson, G. Mallia, D. S. Middlemiss, W. C. Mackrodt, R. Dovesi, R. Orlando, The Performance of Hybrid Density Functionals in Solid State Chemistry, Springer, Berlin **2004** .
[51] J. Muscat, A. Wander, N. M. Harrison, *Chem. Phys. Lett.* **2001**, *342*, 397.
[52] J. P. Perdew, M. Levy, *Phys. Rev. Lett.* **1983**, *51*, 1884.
[53] Y.-H. Li, A. Walsh, S. Chen, W.-J. Yin, J.-H. Yang, J. Li, J. L. F. Da Silva, X. G. Gong, S.-H. Wei, *Appl. Phys. Lett.* **2009**, *94*, 212109.
[54] S. B. Zhang, S.-H. Wei, A. Zunger, *Phys. Rev. Lett.* **2000**, *84*, 1232.
[55] W. Walukiewicz, *Physica B: Condens. Matter* **2001**, *302-303*, 123.
[56] A. Walsh, C. R. A. Catlow, M. Miskufova, A. A. Sokol, *J. Phys.: Condens. Matter* **2011**, *23*, 334217.
[57] J.-H. Yang, S. Chen, W.-J. Yin, X. G. Gong, A. Walsh, S.-H. Wei, *Phys. Rev. B* **2009**, *79*, 245202.
[58] J. Paier, R. Asahi, A. Nagoya, G. Kresse, *Phys. Rev. B* **2009**, *79*, 115126.
[59] M. Ichimura, Y. Nakashima, *Jpn. J. Appl. Phys.* **2009**, *48*, 090202.
[60] Y. Zhang, X. Yuan, X. Sun, B.-C. Shih, P. Zhang, W. Zhang, *Phys. Rev. B* **2011**, *84*, 075127.
[61] H. Zhao, C. Persson, *Thin Solid Films* **2011**, *519*, 7508.
[62] S. Botti, *Appl. Phys. Lett.* **2011**, *98*, 241915.
[63] J. P. Perdew, A. Zunger, *Phys. Rev. B* **1981**, *23*, 5048.
[64] J. P. Perdew, K. Burke, M. Ernzerhof, *Phys. Rev. Lett.* **1996**, *77*, 3865.
[65] S. Chen, A. Walsh, J. H. Yang, X. Gong, L. Sun, P. X. Yang, J. H. Chu, S. H. Wei, *Phys. Rev. B* **2011**, *83*, 125201.
[66] H. Wang, *Int. J. Photoenergy* **2011**, *2011*, 801292.
[67] S. Chen, X. G. Gong, A. Walsh, S.-H. Wei, *Appl. Phys. Lett.* **2010**, *96*, 021902.
[68] S. Chen, J.-H. Yang, X. G. Gong, A. Walsh, S.-H. Wei, *Phys. Rev. B* **2010**, *81*, 245204.
[69] X. Fontane, L. Calvo-Barrio, V. Izquierdo-Roca, E. Saucedo, A. Perez-Rodriguez, J. R. Morante, D. M. Berg, P. J. Dale, S. Siebentritt, *Appl. Phys. Lett.* **2011**, 98.
[70] Y. T. Zhai, S. Chen, J. H. Yang, H. J. Xiang, X. G. Gong, A. Walsh, J. Kang, S. H. Wei, *Phys. Rev. B* **2011**, *84*, 075213.
[71] S. B. Zhang, S.-H. Wei, A. Zunger, H. Katayama-Yoshida, *Phys. Rev. B* **1998**, *57*, 9642.
[72] G.-X. Qian, R. M. Martin, D. J. Chadi, *Phys. Rev. B* **1988**, *38*, 7649.
[73] G. A. Baraff, E. O. Kane, M. Schlüter, *Phys. Rev. B* **1980**, *21*, 5662.
[74] J. Neugebauer, C. G. Van de Walle, *Phys. Rev. B* **1994**, *50*, 8067.
[75] A. Nagoya, R. Asahi, R. Wahl, G. Kresse, *Phys. Rev. B* **2010**, *81*, 113202.
[76] T. Maeda, S. Nakamura, T. Wada, *Jpn. J. Appl. Phys.* **2011**, *50*, 04DP07.
[77] S. Siebentritt, M. Igalson, C. Persson, S. Lany, *Prog. Photovoltaics: Res. Appl.* **2010**, *18*, 390.
[78] K. Hones, E. Zscherpel, J. Scragg, S. Siebentritt, *Physica B: Condens. Matter* **2009**, *404*, 4949.
[79] S. Susan, *Sol. Energy Mater. Sol. Cells* **2011**, *95*, 1482.
[80] S. J. Ahn, S. Jung, J. Gwak, A. Cho, K. Shin, K. Yoon, D. Park, H. Cheong, J. H. Yun, *Appl. Phys. Lett.* **2010**, *97*, 021905.
[81] Q. Guo, G. M. Ford, W. C. Yang, B. C. Walker, E. A. Stach, H. W. Hillhouse, R. Agrawal, *J. Am. Chem. Soc.* **2010**, *132*, 17384.
[82] S.-H. Wei, L. G. Ferreira, J. E. Bernard, A. Zunger, *Phys. Rev. B* **1990**, *42*, 9622.
[83] S. Siebentritt, *Sol. Energy Mater. Sol. Cells* **2011**.
[84] J. Pohl, A. Klein, K. Albe, *Phys. Rev. B* **2011**, *84*, 121201.
[85] J. Pohl, K. Albe, *J. Appl. Phys.* **2010**, *108*, 023509.
[86] A. R. Organov, *Modern Methods of Crystal Structure Prediction*, Wiley-VCH, Weinheim **2011**.
[87] G. Trimarchi, A. Zunger, *Phys. Rev. B* **2007**, *75*, 104113.
[88] S. M. Woodley, R. Catlow, *Nat. Mater.* **2008**, *7*, 937.
[89] D. C. Lonie, E. Zurek, *Comput. Phys. Commun.* **2011**, *182*, 372.
[90] A. Franceschetti, A. Zunger, *Nature* **1999**, *402*, 60.
[91] G. Ceder, Y. M. Chiang, D. Sadoway, M. Aydinol, Y. I. Jang, B. Huang, *Nature* **1998**, *392*, 694.
[92] G. Hautier, C. C. Fischer, A. Jain, T. Mueller, G. Ceder, *Chem. Mater.* **2010**, *22*, 3762.